Materials Advances

PAPER

Check for updates

Ambient pressure synthesis of unstable bulk phases of strongly correlated rare-earth nickelates†

Nicholas Smieszek, [ID] ‡[a] Xinran Li‡[a] and Vidhya Chakrapani [ID] *[ab]

Despite the outstanding electrical, electrochemical, and optical properties of rare-earth (R)-doped nickelates ($RNiO_3$), a bottleneck in its device applications is the need for high-pressure, typically in excess of 100 bars, to stabilize this phase during synthesis. To date, no known near-ambient pressure synthesis process exists for the synthesis of bulk $RNiO_3$ with ionic radii of R lower than that of Nd (such as Sm, Eu, and Gd) in the lanthanide series due to the increasing thermodynamic instability of Ni^{3+} cations at ambient pressures. In the present study, we report a set of conditions for the successful synthesis of bulk $SmNiO_3$ and $NdNiO_3$ through a sol–gel synthesis procedure followed by annealing at ambient pressure to stabilize Ni^{3+}. Rietveld refinement analysis shows the composition of crystalline $SmNiO_3$ and $NdNiO_3$ phases to be as high as 50 wt% and 96 wt%, respectively. Consequently, sharp, well-defined insulator–metal transitions (IMTs) involving resistance changes of 2–3 orders of magnitude could be achieved, which is comparable to that seen in high-pressure synthesized samples reported in the literature.

1. Introduction

Rare-earth nickelates are an important class of functional materials that exhibit a diverse range of remarkable properties and functionalities, such as the observation of size-tunable insulator–metal transitions (IMTs),[1,2] low-temperature superconductivity,[3,4] unusual antiferromagnetic ordering,[5] and strong bifunctional electrocatalytic activity,[6] which can be exploited for advanced optoelectronics,[7] photodetection,[8] neuromorphic and synaptic devices,[9] smart windows, sensors,[10] regenerative fuel cells[11] and other energy storage devices.[12] The flexibility of the perovskite structure of $RNiO_3$ allows for efficient doping of various rare-earth ions, which affects the rotation, tilt, and distortion of the NiO_6 octahedra, which gives rise to tunable structural, electrical, optical and magnetic properties.[13] For instance, the IMT temperature of $RNiO_3$ can be systematically tuned from low to high with the rare-earth ions of decreasing ionic radius, such as 130 K with Pr, 200 K with Nd, 400 K with Sm, and 460 K with Eu in $RNiO_3$.[14]

Unfortunately, the facile bulk synthesis of $RNiO_3$ is currently a bottleneck to both the fundamental studies and exploit its

unique properties in a wider range of device applications. The underlying cause for the synthetic challenge is the difficulty in stabilizing higher valent Ni^{3+} cations in the $RNiO_3$ lattice (except $LaNiO_3$), which is thermodynamically unstable under typical oxide growth conditions at low or ambient pressures.[15] Most reported bulk $RNiO_3$ synthesis methods use high pressure and high temperature conditions of 150 to 60 000 bar of O_2 and 800 to 1000 °C for several days.[1,16] Such extreme conditions require the use of specialized equipment that can neither be developed in a common laboratory nor is readily available commercially. Therefore, developing strategies for low pressure bulk synthesis or stabilization is highly attractive. Thin films can be obtained without extreme annealing conditions through epitaxial stabilization on lattice-matched single crystal substrates.[17–19] However, this condition restricts the thickness of the oxide layer that can be used without the onset of instability as well as the choice of substrates and the type of device that can be employed for experiments.[20]

The difficulty in low-pressure Ni^{3+} stabilization exacerbates as the ionic radius of the rare earth dopant decreases. Thermodynamic analysis by Jaramillo *et al.*[15] shows that the Gibbs free energy of the formation of the $RNiO_3$ phase increases with the decreasing ionic radius of the rare earth dopant. This may be related to the increased bending of the Ni–O–Ni bond angle, defined in terms of the tolerance factor (t), occurring in $RNiO_3$ phases with smaller size R atoms, which may affect the cohesive energy of the crystal lattice. Table 1 summarizes the reported experimental conditions commonly employed for the

[a] Howard P. Isermann Department of Chemical and Biological Engineering, Rensselaer Polytechnic Institute, Troy, New York-12180, USA

[b] Department of Physics, Applied Physics, and Astronomy, Rensselaer Polytechnic Institute, Troy, New York-12180, USA. E-mail: chakrv@rpi.edu

† Electronic supplementary information (ESI) available. See DOI: https://doi.org/10.1039/d2ma00415a

‡ Equal contribution.

Table 1 Summary of the reported experimental conditions commonly employed for the synthesis of some bulk nickelate phases

Bulk phase	Ambient pressure synthesis?	Synthesis method and conditions	Ref.
$LaNiO_3$	Yes	Solid-state flux method at 800 °C for 72 h or 1300 °C for 48 h in air	21
		Electrospinning + annealing at 950 °C for 1 h	12
$PrNiO_{3-\delta}$	Yes	Solid-state nitrate annealing at 850 °C for 48 h under O_2 flow	22,27
$NdNiO_3$	Yes	Sol–gel precipitation and annealing at 650 °C in O_2 for 5 days	23
		Hydrothermal synthesis + annealing at 400 °C for 3 h.	25
		Electrospinning + annealing at 800 °C under O_2 flow for 4 h	26
		High pressure synthesis $NdNiO_{3-\delta}$: solid state precursor/sol gel preparation + annealing at 50 bar O_2 for 25 h	33
$SmNiO_3$	No	High pressure synthesis Non-stoichiometric oxygen deficient: Solid state precursor/ solgel preparation + 900 °C annealing at 50 bar O_2 for 25 h	33
		Stoichiometric: solid state precursor/sol gel preparation + 1000 °C annealing at 150–200 bar O_2 for several days	16
$EuNiO_3$ and other $RNiO_3$	No	$EuNiO_3$: Solid state precursor/sol gel preparation + 1000 °C annealing at 200 bar O_2 for 3 days	14
		Others: Solid state precursor/sol gel preparation + 950 °C annealing at 60 000 bar O_2 for 12 minutes	1

synthesis of several bulk nickelate phases. The near-ambient pressure syntheses of bulk and nanostructured La-,[21] Pr-[22] and Nd[23–25]-doped $RNiO_3$ have been reported through several techniques, such as the solid-state flux method,[21] solid-state nitrate annealing,[22] sol–gel precipitation and annealing,[23] electrospinning,[26] and hydrothermal synthesis.[25] However, no report exists for the low-pressure synthesis of nickelates with rare earth elements past Nd in the lanthanide series (such as Sm, Eu, *etc.*). This is consistent with the phase diagrams reported by Jaramillo *et al.*[15] for Pr-, Nd-, and $SmNiO_3$, which indicate that the lowest O_2 partial pressures required for the thermodynamic stabilization of the $RNiO_3$ phase at a typical synthesis temperature of 700 °C are 10^{-2} bar, 1.2 bar, and 180 bar, respectively. Vibhu *et al.*[27] reported that annealing citrate sol–gel of precursors at 850 °C for 48 h under oxygen flow synthesis can produce oxygen-deficient $PrNiO_{3-\delta}$. The phase was reported to be stable up to 950 °C in ambient air. Similarly, Tiwari and Rajeev[28] reported the successful synthesis of the nearly stoichiometric composition of $NdNiO_{2.92}$ with continuous annealing of sol–gel synthesized pellets at 800 °C in O_2 at ambient pressure for 7 days. However, no synthesis condition exists for the ambient-pressure preparation of bulk $SmNiO_3$. In the present study, we report two aging protocols to stabilize Ni^{3+} without the need for high-pressure annealing conditions. Our results show that both $SmNiO_3$ and $NdNiO_3$ phases can be crystallized/stabilized through either a high temperature aging process in the temperature range of 650–700 °C for 1–3 weeks or *via* slow aging of the as-synthesized sub-stoichiometric phase in ambient air for 6–8 months. Both conditions lead to an increase in the crystalline $RNiO_3$ content of the lattice and give rise to sharp insulator-to-metal transitions involving a resistance change of at least 2–3 orders of magnitude.

2. Experimental

Bulk nickelates of Sm and Nd doping were synthesized using a modified sol–gel method of Vassiliou *et al.*,[23] which involved dissolving $Sm(NO_3)_3 \cdot 6H_2O$ or $Nd(NO_3)_3 \cdot 6H_2O$ along with $Ni(NO_3)_2 \cdot 6H_2O$ and citric acid in 100 mL of deionized water in a 1:1:1.67 molar ratio. Next, 1.5 mL of 0.5 M ethylenediaminetetraacetic acid (EDTA) was added, and the pH was adjusted to 7 using NH_4OH. The solution was heated to 80 °C with constant stirring until most of the water evaporated and a gel was formed. The resulting gel was dried at 100 °C for 12 hours, ground into a powder, and further annealed at 400 °C for 6 hrs. The resulting powder was pelletized under 4 metric tons of force for 10 minutes and subsequently annealed again at 700 °C for 12 hours.

The composition of the nickelate pellets was determined by X-ray diffraction (XRD), which was recorded using a PANalytic X'Pert Pro diffractometer using Cu K_α radiation. We applied the Rietveld refinement to the diffraction patterns using the FULL-PROF program and the theoretically-calculated diffraction patterns of possible phases from the Materials Project Database. Metal–insulator transitions were recorded by measuring the two-probe resistance on the sintered pellets using a home-built liquid nitrogen-cooled temperature stage.

3. Results and discussion

Fig. 1a and b show the resistance profiles of as-synthesized Nd-doped ($NdNiO_x$) and Sm-doped ($SmNiO_x$) nickelate pellets as a function of temperature, respectively. Neither samples exhibit a sharp temperature-induced IMT at expected temperatures of ~ 200 K and 400 K, respectively. However, such a profile is similar to that reported in the literature for these nickelates synthesized under low pressure conditions.[6,15] The composition of the crystalline phases of the as-synthesized pellets was determined by the Rietveld refinements of the measured XRD patterns and is shown in Fig. 1c and d. The fitting parameters and results are summarized in Table S1 in the ESI.† The points in the spectra represent the experimental data while the solid lines correspond to the fitted pattern. The green bars under the coordinate system are the calculated Bragg positions of different phases. The 'noise-like' curve below the green bars represents the difference between the experimental and calculated data. The refinement results show that the predominant
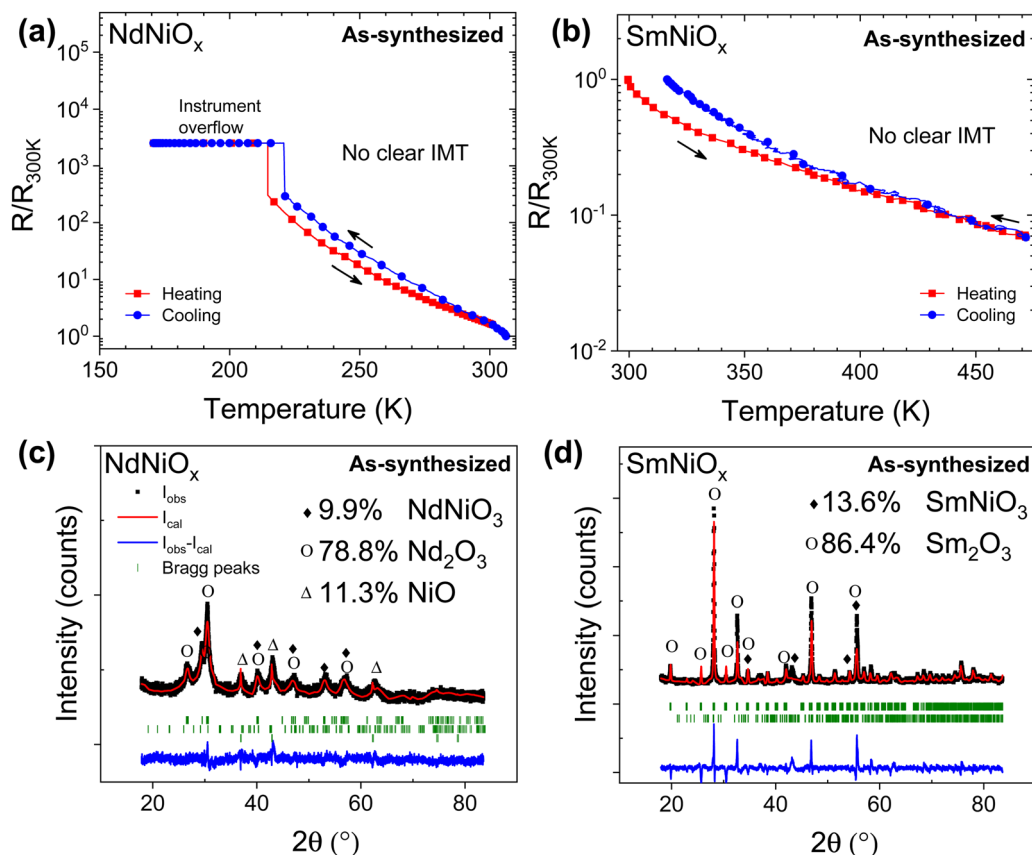
Fig. 1 (a and b) Normalized electrical resistances of Nd-doped (NdNiO$_x$) (a) and Sm-doped (SmNiO$_x$) (b) nickelate pellets as a function of temperature. R_{300K} is the resistance measured at room temperature. (c and d) Rietveld-refined X-ray powder diffraction patterns obtained at room temperature of NdNiO$_x$ (c) and SmNiO$_x$ (d). Circles and the continuous lines represent the experimental and calculated spectra, respectively, and their difference is shown in the bottom curve. The vertical ticks are the 2θ Bragg positions.

crystalline phase in the as-synthesized pellet is the cubic Sm$_2$O$_3$ and trigonal Nd$_2$O$_3$ phases in Sm-doped and Nd-doped nickelate pellets, respectively, with only 10–15% of the RNiO$_3$ phase. It is likely that at the low synthesis temperature, either the RNiO$_3$ phase formation was not completed within the synthesis time due to the difficulty in stabilizing Ni^{3+} or the as-formed RNiO$_3$ phase is amorphous and, therefore, not detectable by XRD. The latter is very likely to have occurred because the composition of crystalline phases does not account for the total Ni content of the sample.

To promote the crystallization of the RNiO$_3$ phase, we tested the effect of aging on the as-synthesized pellets using two methods, which involved: (i) high temperature (HT) aging from 650 °C to 700 °C for 1–3 weeks under ambient air and (ii) aging of the pellets at room temperature (RT) in a laboratory air environment for 6–8 months, followed by annealing at 700 °C for 12 hours. The compositional and electrical characteristics of both sets of samples were determined, which are summarized in Fig. 2 and 3 and Table 2. According to the Rietveld refinement of the XRD patterns, the crystalline RNiO$_3$ content in both Sm- and Nd-doped samples increased with aging under both sets of conditions. In Nd-doped pellet (NdNiO$_x$), the weight percent of the crystalline NdNiO$_3$ phase increased from ∼10%

in the as-synthesized sample to 53% with aging at RT (Fig. 2a). However, a higher improvement was seen in samples that underwent HT aging, wherein the crystalline NdNiO$_3$ concentration increased from 10% to 61.7% after 7 days of continuous annealing and further increased to 96.2% upon annealing for two additional weeks (Fig. 2b). Thus, nearly phase-pure, fully crystallized NdNiO$_3$ can be achieved through accelerated aging without the need for high-pressure annealing conditions. The obtained RNiO$_3$ phase is likely oxygen-deficient. This result confirms the prior work of Tiwari and Rajeev,[28] who reported the successful synthesis of the nearly stoichiometric composition of NdNiO$_{2.92}$ with continuous annealing of sol–gel synthesized pellets at 800 °C in an O$_2$ environment at ambient pressure for 7 days. The diffractogram indicates the sample to consist of an orthorhombically distorted perovskite structure with a *Pnma* space group symmetry. The refined lattice parameters were $a = 5.41635$ Å, $b = 5.55054$ Å, and $c = 7.68114$ Å.[3] These values are very close to but slightly greater than values observed in high-pressure synthesized bulk samples whose values are $a = 5.3891$ Å, $b = 5.3816$ Å and $c = 7.6101$ Å.[1]

With the increase in the NdNiO$_3$ content, the aged Nd-doped sample showed a well-defined and sharp IMT at temperatures between 140 K and 180 K with more than 4 orders of magnitude
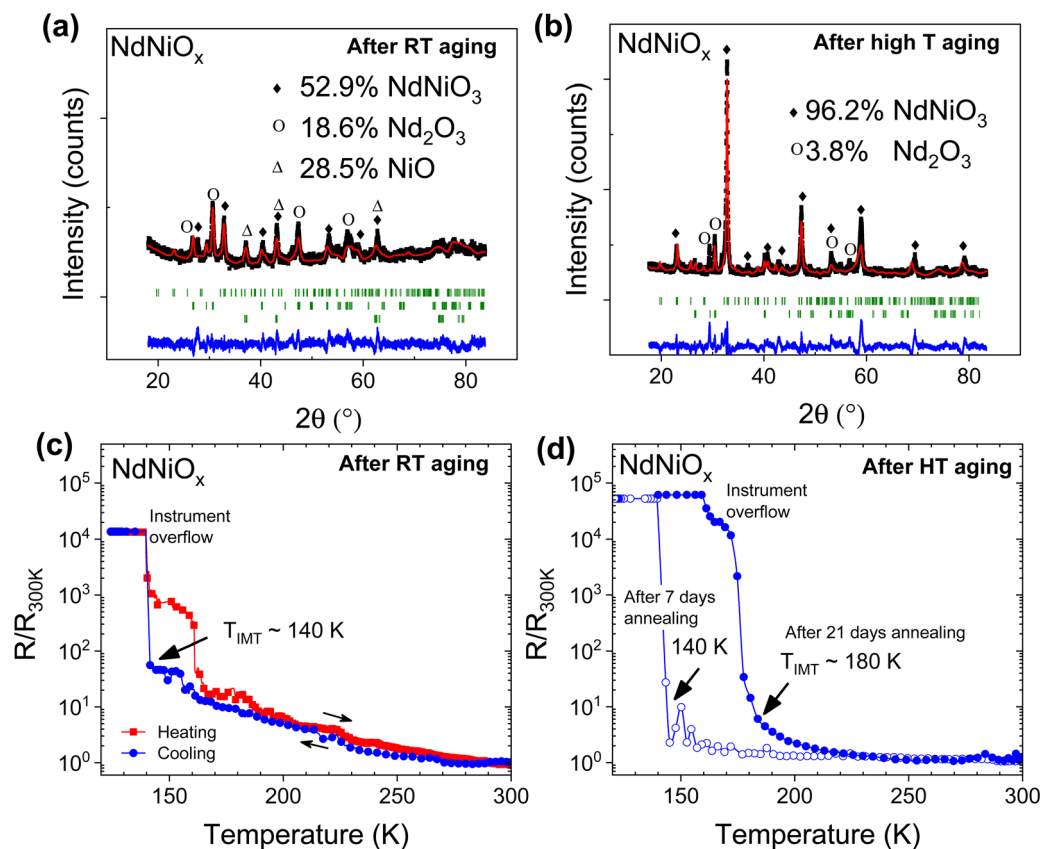
Fig. 2 (a and b) Room temperature Rietveld-refined X-ray powder diffraction patterns of Nd-doped nickelate pellets after room temperature aging (a) and high-temperature aging at 650 °C for 3 weeks (b). (c and d) Normalized electrical resistances of RT-aged (c) and HT-aged (d) Nd-doped nickelate pellets as a function of temperature showing sharp IMT characteristics.

change in the electrical resistance (Fig. 2c and d). In both the RT-aged sample and the HT aged sample that were annealed for 7 days, the T_{IMT} occurred at 140 K. However, in the HT-aged sample with the highest $NdNiO_3$ content of 96%, the T_{IMT} occurred at 180 K, which is close to the 180–200 K reported in earlier studies.[14,28]

Similar to $NdNiO_x$, both aging methods led to a substantial increase in the $SmNiO_3$ concentration in Sm-doped pellets (Fig. 3a and b). The weight percent of $SmNiO_3$ increased from ~14% in the as-synthesized sample to 43% with aging at RT and to 34% upon HT-annealing at 650 °C for 1 week. The Rietveld fitting analysis indicates that a monoclinic (mn) Sm_2O_3 phase at a concentration of 13.1% may be present along with cubic (c) Sm_2O_3 (44%) in RT-aged Sm-doped pellets. Increasing the annealing time to 4 weeks did not significantly increase the composition of $SmNiO_3$ (39.7%). Instead, it was found that annealing at 700 °C for 9 days could increase the $RNiO_3$ composition close to 50%. The XRD refinement results indicate that this $SmNiO_3$ phase consists of an orthorhombically distorted perovskite structure with a *Pnma* space group symmetry (Fig. 3a and b). The refined lattice parameters were $a = 5.8256$ Å, $b = 4.9550$ Å, and $c = 7.7341$ Å, which are somewhat higher than the values of $a = 5.3283$ Å, $b = 5.4374$ Å and $c = 7.5675$ Å reported for high-pressure synthesized bulk

$SmNiO_3$.[16] The lower wt% of $RNiO_3$ in Sm-doped pellets compared to Nd-doped pellets after aging points to the increasing difficulty in stabilizing Ni^{3+} as the ionic radius of the rare-earth dopant decreases. Furthermore, $SmNiO_3$ also required a longer aging time of 6 to 8 months for stabilization, while $NdNiO_3$ required a RT aging time of only 1 to 4 weeks. Attempts at decreasing the aging time by either increasing or decreasing the ambient humidity had no effect on the aging process (data not shown). Despite the mixed phase with a lower $RNiO_3$ content compared to that seen in Nd-doped pellets, aged Sm-doped pellets showed a very well-defined and sharp IMT at temperatures between 400 K and 420 K (Fig. 3c and d) with a resistance change of 10^2–10^3, which is comparable to the 10^2 resistance change seen for high-pressure synthesized bulk[16] and thin films.[15]

While the XRD results indicate the formation of the crystalline $RNiO_3$ phase with aging, X-ray photoemission spectroscopy (XPS) was performed to confirm the increase in the Ni^{3+} content. Unlike XRD that only probes the crystalline phases, composition changes probed through XPS reflect changes in both amorphous and crystalline phases. Fig. 4 compares the Ni $2p_{3/2}$ core-level XPS spectrum of as-synthesized and aged Nd- and Sm-doped pellets. The extrinsic loss structure of each spectrum was subtracted using a Shirley-type correction. The Ni $2p_{3/2}$ peak was fit using multiplet envelope peaks of
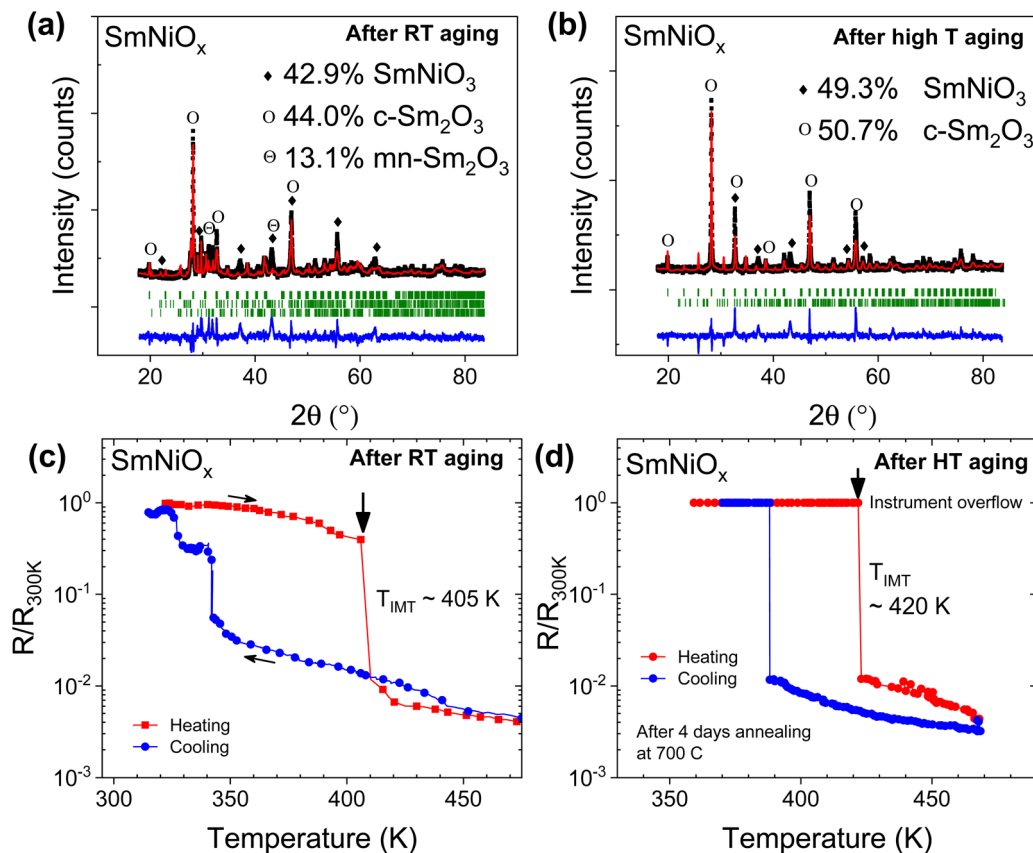
Fig. 3 (a and b) Room temperature Rietveld-refined X-ray powder diffraction patterns of Sm-doped nickelate pellets after room temperature aging (a) and high-temperature aging at 650 °C (b). (c and d) Normalized electrical resistances of RT-aged (c) and HT-aged (d) of Sm-doped nickelate pellets as a function of temperature showing sharp IMT characteristics.

Table 2 Summary of the compositional analysis of the crystalline phases of Nd- and Sm-doped nickelate pellets prepared under different experimental annealing conditions

Annealing conditions	% of RNiO₃ (R = Nd or Sm)	% of R₂O₃	% of NiO
NdNiO$_x$			
Pristine	9.9	78.8	11.3
RT aging	52.9	28.5	28.52
650 °C for 7 days	64.4	35.6	
650 °C for 7 + 14 days	96.2	3.8	
SmNiO$_x$			
Pristine	13.64	86.36	
RT aging	42.9	57.1	
650 °C for 7 days	34.13	65.87	
650 °C for 7 + 14 days	30.60	69.40	
650 °C for 28 days	39.71	60.29	
700 °C for 4 days	43.18	56.82	
700 °C for 4 + 5 days	49.31	50.69	

theoretically predicted[29,30] free Ni^{2+} and Ni^{3+} ions using the previously reported procedure of Biesinger et al.[31] and Qi et al.[32] Fitting was performed by constraining both the binding energy (BE) positions and the full-width-at-the-half maximum (FWHM) of the peaks to the same values between different spectra, and is summarized in Table S2 in the ESI.† In mixed-valent nickel oxides, the predominant Ni^{2+} peaks appear at a lower BE (853.7) while the peaks of Ni^{3+} occur at higher BEs (854.6, 855.3, and 856.5 eV).[31]

The multiplet-fitting analysis shows that the Ni^{3+} contents of Nd- and Sm-doped pellets increase with both RT- and HT-aging. In RT-aged Nd-doped pellet, the Ni^{3+}/Ni^{2+} ratio increased modestly from 2.2 to 2.6. In this sample, XRD analysis indicated an increase in the $NdNiO_3$ content from 9% to 52.9%. However, a larger increase in the Ni^{3+}/Ni^{2+} concentration ratio from 1.2 to 3.5 was observed in the Sm-doped sample, in which XRD analysis showed an increase in the $SmNiO_3$ content from 13.6% to 49.3%. In line with this, the O/Ni ratio in Sm-doped pellet increased by 160% after HT-aging. We note that the particulate nature of the samples in the present study prevented the evaluation of relative changes in the Ni and O stoichiometry from the integrated peak areas. However, the comparative analysis of the O/Ni ratio between pristine and aged samples can still be performed. These results suggest that aging promotes both the formation of $RNiO_3$ and crystallization of amorphous $RNiO_3$ present in the as-synthesized sample, and thus lead to an increase in the Ni^{3+} content relative to the Ni^{2+} content through oxygen incorporation into the lattice. The valence band (VB) spectra of both as-synthesized and aged samples show them to be p-type semiconductors (Fig. S1 in the ESI†).

Based on the XRD and XPS results, we briefly consider the mechanism of $RNiO_3$ stabilization. The formation/decomposition reaction of $RNiO_3$ can be written as

$$0.5R_2O_3 + Ni^{2+}O + 0.25O_2 \leftrightarrow RNi^{3+}O_3 \quad (R1)$$
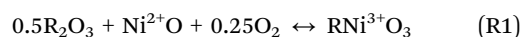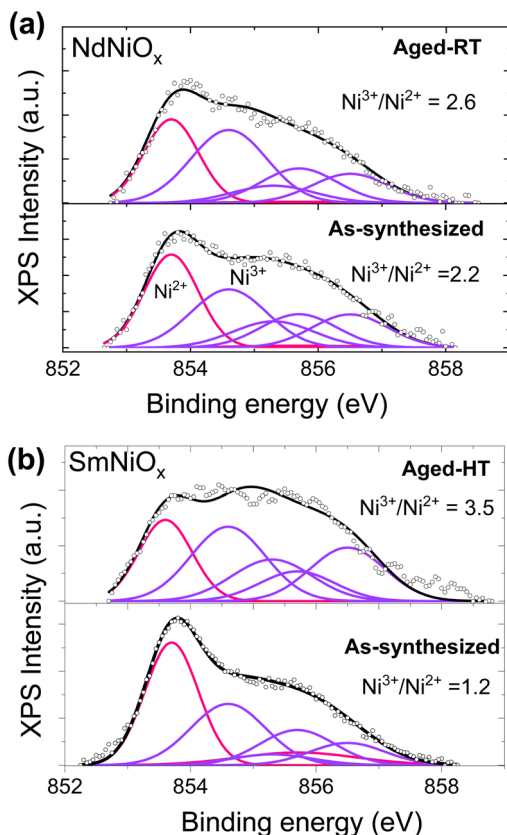
Fig. 4 XPS spectra of the Ni $2p_{3/2}$ core-level spectra of Nd-doped (a) and Sm-doped nickelate pellets (b) before and after aging. Each spectrum was fitted with Ni^{2+} and Ni^{3+} multiplet envelopes using the procedure of Biesinger et al.[31] The summary of the fitting analysis of the fitted peaks and their peak energy positions, areas, and FWHMs is given in Table S2 in the ESI.†

While the Rietveld analysis indicates the presence of only a low concentration of $RNiO_3$ in the as-synthesized samples, stoichiometric consideration suggests that Ni is likely present as an amorphous phase, such as in NiO or $RNiO_3$. Based on their systematic annealing studies at high O_2 pressures of 100 bar, Jaramillo et al.[15] suggested that recrystallization of the $SmNiO_3$ amorphous phase is the rate-limiting step at sufficiently high oxygen partial pressure due to the slow cation diffusion in the mixed phase matrix. This may not be the case in the present scenario where annealing was carried out at ambient pressure in an air environment. Therefore, it is likely that oxygen incorporation is the rate limiting step. In particular, we point to the results of Tiwari and Rajeev,[28] who studied the formation of oxygen deficient $NdNiO_{3-\delta}$ through the systematic variation in the oxygen partial pressure during growth. The lower oxygen concentration in the gas phase was shown to destabilize the $NdNiO_3$ phase, which resulted in the formation of the oxygen deficient phase with a lower Ni–O–Ni bond angle and higher T_{IMT}. $NdNiO_{3-\delta}$ was shown to be no longer stable for $x > 0.22$. Therefore, oxygenation may be the key step in stabilizing the $RNiO_3$ phase, which is consistent with the results presented in this study. In contrast, oxygen deficiency likely promotes the

$RNiO_3$ decomposition to R_2O_3 and NiO (reverse of Reaction (1)), which may be the reason for the observed R_2O_3 phase and possible amorphous NiO phase in the as-synthesized samples.

4. Conclusion

In summary, ambient-pressure aging, involving either a slow ambient-air oxidation for 6–8 months or an accelerated aging at a higher temperature of 650 °C for 1–3 weeks, of bulk Sm-doped and Nd-doped nickelate pellets prepared by the conventional solid-state preparation technique can stabilize Ni^{3+} and form the $RNiO_3$ phase. The Rietveld refinement analysis of crystalline phases shows a composition as high as 96 wt% of $NdNiO_3$ and 49.3 wt% of $SmNiO_3$ can be obtained through aging. Consequently, sharp well-defined insulator-to-metal transitions (IMTs) involving resistance changes of 10^2–10^3 could be achieved in mixed-phase samples, which is comparable to that seen in high-pressure synthesized samples, and may be of practical importance in many device applications. Further work is needed to explore how aging helps in stabilizing nickelates doped with R cations of even lower ionic radii than Sm, such as Eu and Y, and are currently underway. The preliminary results indicate that they require even longer annealing time, spanning several weeks, than $SmNiO_3$ for stabilization.

Data availability

The data that support the findings of this study are available from the corresponding author upon reasonable request.

Author contributions

N. S. and X. L. performed the experiments. V. C. wrote the manuscript. All the authors contributed towards data analysis and manuscript preparation.

Conflicts of interest

All the authors declare that they have no conflicts of interest.

Acknowledgements

References

1 G. Demazeau, A. Marbeuf, M. Pouchard and P. Hagenmuller, *J. Solid State Chem.*, 1971, **3**, 582–589.
2 M. L. Medarde, *J. Phys.: Condens. Matter*, 1997, **9**, 1679.

3 J. Chaloupka and G. Khaliullin, *Phys. Rev. Lett.*, 2008, **100**, 016404.

4 D. Li, K. Lee, B. Y. Wang, M. Osada, S. Crossley, H. R. Lee, Y. Cui, Y. Hikita and H. Y. Hwang, *Nature*, 2019, **572**, 624–627.

5 V. Scagnoli, U. Staub, A. Mulders, M. Janousch, G. Meijer, G. Hammerl, J. Tonnerre and N. Stojic, *Phys. Rev. B: Condens. Matter Mater. Phys.*, 2006, **73**, 100409.

6 L. Wang, K. A. Stoerzinger, L. Chang, J. Zhao, Y. Li, C. S. Tang, X. Yin, M. E. Bowden, Z. Yang and H. Guo, *Adv. Funct. Mater.*, 2018, **28**, 1803712.

7 Z. Li, Y. Zhou, H. Qi, Q. Pan, Z. Zhang, N. N. Shi, M. Lu, A. Stein, C. Y. Li, S. Ramanathan and N. Yu, *Adv. Mater.*, 2016, **28**, 9117–9125.

8 L. Wang, L. Chang, X. Yin, L. You, J.-L. Zhao, H. Guo, K. Jin, K. Ibrahim, J. Wang, A. Rusydi and J. Wang, *Appl. Phys. Lett.*, 2017, **110**, 043504.

9 J. Shi, S. D. Ha, Y. Zhou, F. Schoofs and S. Ramanathan, *Nat. Commun.*, 2013, **4**, 2676.

10 L. Xuchen, X. Tingxian and D. Xianghong, *Sens. Actuators, B*, 2000, **67**, 24–28.

11 R. N. Singh, A. N. Jain, S. K. Tiwari, G. Poillerat and P. Chartier, *J. Appl. Electrochem.*, 1995, **25**, 1133–1138.

12 D. K. Hwang, S. Kim, J.-H. Lee, I.-S. Hwang and I.-D. Kim, *J. Mater. Chem.*, 2011, **21**, 1959–1965.

13 J. B. Goodenough, *Rep. Prog. Phys.*, 2004, **67**, 1915–1993.

14 J. B. Torrance, P. Lacorre, A. I. Nazzal, E. J. Ansaldo and C. Niedermayer, *Phys. Rev. B: Condens. Matter Mater. Phys.*, 1992, **45**, 8209–8212.

15 R. Jaramillo, F. Schoofs, S. D. Ha and S. Ramanathan, *J. Mater. Chem. C*, 2013, **1**, 2455–2462.

16 P. Lacorre, J. B. Torrance, J. Pannetier, A. I. Nazzal, P. W. Wang and T. C. Huang, *J. Solid State Chem.*, 1991, **91**, 225–237.

17 M. A. Novojilov, O. Y. Gorbenko, I. E. Graboy, A. R. Kaul, H. W. Zandbergen, N. A. Babushkina and L. M. Belova, *Appl. Phys. Lett.*, 2000, **76**, 2041–2043.

18 A. Kaul, O. Gorbenko, I. Graboy, M. Novojilov, A. Bosak, A. Kamenev, S. Antonov, I. Nikulin, A. Mikhaylov and M. Kartavtzeva, *MRS Proc.*, 2011, **755**, DD7.1.

19 A. A. Bosak, A. A. Kamenev, I. E. Graboy, S. V. Antonov, O. Y. Gorbenko, A. R. Kaul, C. Dubourdieu, J. P. Senateur, V. L. Svechnikov and H. W. Zandbergen, *Thin Solid Films*, 2001, **400**, 149–153.

20 C. Girardot, S. Pignard, F. Weiss and J. Kreisel, *Appl. Phys. Lett.*, 2011, **98**, 241903.

21 A. Wold, B. Post and E. Banks, *J. Am. Chem. Soc.*, 1957, **79**, 4911–4913.

22 V. Vibhu, A. Flura, A. Rougier, C. Nicollet, S. Fourcade, T. Hungria, J.-C. Grenier and J.-M. Bassat, *J. Energy Chem.*, 2020, **46**, 62–70.

23 J. K. Vassiliou, M. Hornbostel, R. Ziebarth and F. J. Disalvo, *J. Solid State Chem.*, 1989, **81**, 208–216.

24 S. Kim, D. H. Truyen, T. H. Kim and C. W. Bark, *J. Nanosci. Nanotechnol.*, 2020, **20**, 4239–4243.

25 M. Sivakumar, K. Pandi, S.-M. Chen, Y.-H. Cheng and M. Sakthivel, *New J. Chem.*, 2017, **41**, 11201–11207.

26 M. S. Medina, B. N. Ramirez, P. M. G. L. Ferreira, H. P. Huang, A. Zenatti, A. J. C. Lanfredi and M. T. Escote, *Nano Express*, 2020, **1**, 010028.

27 V. Vibhu, A. Flura, C. Nicollet, S. Fourcade, N. Penin, J.-M. Bassat, J.-C. Grenier, A. Rougier and M. Pouchard, *Solid State Sci.*, 2018, **81**, 26–31.

28 A. Tiwari and K. P. Rajeev, *Solid State Commun.*, 1998, **109**, 119–124.

29 R. P. Gupta and S. K. Sen, *Phys. Rev. B: Condens. Matter Mater. Phys.*, 1974, **10**, 71–77.

30 R. P. Gupta and S. K. Sen, *Phys. Rev. B: Condens. Matter Mater. Phys.*, 1975, **12**, 15–19.

31 M. C. Biesinger, B. P. Payne, L. W. M. Lau, A. Gerson and R. S. C. Smart, *Surf. Interface Anal.*, 2009, **41**, 324–332.

32 Q. Wang, A. Puntambekar and V. Chakrapani, *Nano Lett.*, 2016, **16**, 7067–7077.

33 I. V. Nikulin, M. A. Novojilov, A. R. Kaul, S. N. Mudretsova and S. V. Kondrashov, *Mater. Res. Bull.*, 2004, **39**, 775–791.